Smart Structures and Systems, *Vol. 18, No. 6 (2016) 1169-1188*
DOI: http://dx.doi.org/10.12989/sss.2016.18.6.1169

Control strategy for the substructuring testing systems to simulate soil-structure interaction

Jun Guo, Zhenyun Tang*, Shicai Chen and Zhenbao Li

The Key Laboratory of Urban Security and Disaster Engineering, Ministry of Education, Beijing University of Technology. Beijing, 100124, China

(Received October 14, 2015, Revised August 22, 2016, Accepted August 28, 2016)

Abstract. Real-time substructuring techniques are currently an advanced experimental method for testing large size specimens in the laboratory. In dynamic substructuring, the whole tested system is split into two linked parts, the part of particular interest or nonlinearity, which is tested physically, and the remanding part which is tested numerically. To achieve near-perfect synchronization of the interface response between the physical specimen and the numerical model, a good controller is needed to compensate for transfer system dynamics, nonlinearities, uncertainties and time-varying parameters within the physical substructures. This paper presents the substructuring approach and control performance of the linear and the adaptive controllers for testing the dynamic characteristics of soil-structure-interaction system (SSI). This is difficult to emulate as an entire system in the laboratory because of the size and power supply limitations of the experimental facilities. A modified linear substructuring controller (MLSC) is proposed to replace the linear substructuring controller (LSC).The MLSC doesn't require the accurate mathematical model of the physical structure that is required by the LSC. The effects of parameter identification errors of physical structure and the shaking table on the control performance of the MLSC are analysed. An adaptive controller was designed to compensate for the errors from the simplification of the physical model in the MLSC, and from parameter identification errors. Comparative simulation and experimental tests were then performed to evaluate the performance of the MLSC and the adaptive controller.

Keywords: soil-structure-interaction; dynamic substructuring; linear substructuring control; identification errors; adaptive control

1. Introduction

Soil structure interaction (SSI) has been investigated for more than one hundred years. A lot of theoretical research (Wolf 1985, Mylonakis and Gazetas 2000, Medina, Aznarez *et al.* 2013) shows that SSI can be beneficial as well as detrimental to structures; however these conclusions were not successfully verified by experiment, because of the lack of adequate testing facilities and techniques. The primary experimental techniques for SSI are holistic. They include small and large scale models that take both soil and superstructure as specimens. In the large scale models, the large size (even full size) test specimen is built outdoors (Shang, Zhang *et al.* 2007) as a real structure to ensure the reality of the SSI system. Because no strong excitation can be imposed on

*Corresponding author, Assistant Professor, E-mail: tzy@bjut.edu.cn

Copyright © 2016 Techno-Press, Ltd.
http://www.techno-press.org/?journal=sss&subpage=8 ISSN: 1738-1584 (Print), 1738-1991 (Online)

the SSI system; this can only test the effect of SSI on the natural characteristics of structure, such as frequency and damping, in the small scale models, the semi-infinite soil is simulated using a soil box (Chen, Lü *et al*. 2006, Pitilakis, Dietz *et al*. 2008). The whole SSI system can be tested using a shaking table to simulate the seismic excitation. The structures in civil engineering are huge, and the soil box required needs to be much bigger than the superstructure (Chen, Lü *et al*. 2006, Pitilakis, Dietz *et al*. 2008). So the size and power of the testing facilities limit the size of the scale models. The limited size of the model creates significant scaling effects. A novel solution is supplied by real-time dynamic substructuring (RTDS) (Nakashima, Kato *et al*. 1992) to overcome the disadvantages of the holistic method. In substructuring, the whole system is divided into two coupled parts. The part of particular interest or nonlinearity is tested physically. The other part behaves linearly, and is tested numerically. The most important advantage of substructuring is that the specimen can be sized according to the limit of the power of the testing equipment. This makes possible the use of large size components (or even prototype tests). Taking the soil-foundation system (Konagai and Ahsan 2002, Wang, Wang *et al*. 2011) and superstructure as numerical model (Heath, Darby *et al*. 2008), real-time substructure testing for SSI was also realized to simulate the SSI effect on frame (Wang, Wang *et al*. 2011) and bridge (Yan, Li *et al*. 2014).

The key point of substructuring is to reproduce the numerical response of the substructure interface by transfer systems (actuator or shaking table).To ensure the test results are close to those obtained from directly testing the overall system, an adaptable controller (Horiuchi, Inoue *et al*. 1999, Horiuchi and Konno 2001, Zhu, Wang *et al*. 2014, Wallace, Wagg *et al*. 2005) is expected to compensate for transfer systems dynamics, nonlinearities, uncertainties and time-varying parameters within the physical substructures (PS) and transfer system (TS).

Until recently, inverse compensation (Horiuchi, Inoue *et al*. 1999, Horiuchi and Konno 2001, Zhu, Wang *et al*. 2014, Wallace, Wagg *et al*. 2005, Chen, Chang *et al*. 2015) was the commonly used method for substructuring control. However, this method has two limitations. First, accurate estimation of the transfer function or delay is required. The estimation errors of the transfer function may cause poor performance, even instability (Chen and Ricles 2009, Enokida, Stoten *et al*. 2015). Second, the inverse compensation method does not considerate the physical model. The interaction between the physical substructure and the transfer system is inevitable. Only small mass physical models or structural components can be tested using real-time substructuring. A linear substructuring controller (LSC) (Stoten *et al*. 2007, Stoten and Hyde 2006) was proposed to overcome the interaction. The physical substructure of the LSC is taken as the control plant together with the transfer system. A series of adaptive controllers (Stoten, Lim *et al*. 2007, Stoten and Hyde 2006, Stoten, Tu *et al*. 2009, Tu, Lin *et al*. 2010, Neild, Stoten *et al*. 2005) were developed to compensate for the estimation errors, strong nonlinearity, uncertainties and time-varying parameters of transfer systems and the physical model. The performance was found to be satisfactory (Tu, Lin *et al*. 2010, Neild, Stoten *et al*. 2005).

In SSI testing systems using RTDS, the specimens (superstructures) are always large and complex. The LSC together with the adaptive controllers is suitable for this system. The only drawback is that the transfer function of the physical model is needed in LSC, but structures in civil engineering are complicated systems with tens of degrees of freedom (DOFs). The undesirable high-order transfer function and the numerous parameters that need to be identified are inevitable. Therefore, a modified LSC controller (MLCS) for SSI systems is necessary. The system identification errors of TS and PS are also inescapable, and this part of effects are planned to be compensated by the adaptive minimal control synthesis algorithm with error feedback (MCSEF)

algorithm. Section 2 describes the RTDS scheme of SSI. The control strategies of RTDS for SSI system are developed with the combination of MLSC and MCSEF and their performance are discussed in Section 3. Comparative simulation tests of the developed control strategies are performed to show the control performance in section 4. In section 5 an experimental test is described to verify the validity of the MLSC-MCSEF controlled RTDS system to simulate SSI effect. Section 6 summarizes the conclusions.

2. The RTDS scheme for SSI systems

In the monolithic model of SSI system often used in civil engineering applications, the superstructure and its foundation together with the soil in its vicinity are used to describe the SSI systems with all the nonlinearities of material (irreversible soil behaviour, sliding along the interface) or geometric origin (uplift of the foundation). These descriptions of the SSI system are complex and computationally expensive. To simplify the complexity of the foundation-soil system, different numerical models (Wolf 1985, Luan and Lin 1996, Chatzigogos, Pecker *et al*. 2009) were developed .The simplified models make it easier to analyse global SSI systems numerically and provide an opportunity to evolve a novel method based on substructuring to investigate SSI experimentally. The lumped-parameters model (LPM) (Luan and Lin 1996) was chosen for the development of SSI substructuring herein. In this model shown in Fig. 1, only the lateral movement of SSI system is considered. The soil-foundation system is represented by a two DOFs system, with two mass blocks (m_{f1},m_{f2}), three springs (k_{f1},k_{f2},k_{f3}) and three dashpots(c_{f1},c_{f2},c_{f3}). The mass ($\mathbf{M}_f$), damping ($\mathbf{C}_f$) and stiffness ($\mathbf{K}_f$) matrices of this system are governed by

$$\mathbf{M}_f = M_{fe}\begin{bmatrix} m_{f1}^* & \\ & m_{f2}^* \end{bmatrix}, \mathbf{C}_f = C_{fe}\begin{bmatrix} c_{f1}^*+c_{f2}^* & -c_{f2}^* \\ -c_{f2}^* & c_{f2}^*+c_{f3}^* \end{bmatrix}, \mathbf{K}_f = K_{fe}\begin{bmatrix} k_{f1}^*+k_{f2}^* & -k_{f2}^* \\ -k_{f2}^* & k_{f2}^*+k_{f3}^* \end{bmatrix} \quad (1)$$

where M_{fe}, C_{fe} and K_{fe} are the unified mass, damping and stiffness respectively. In case of strip footing on an elastic foundation, the unified parameters can be obtained from the following equations (Luan and Lin 1996)

$$K_{fe} = K_s = \frac{8\rho v_s^2 r_0}{2-\nu}, C_{fe} = K_s\frac{r_0}{v_s}, K_{fe} = K_s\left(\frac{r_0}{v_s}\right)^2 \quad (2)$$

where K_s is the static stiffness, v_s is the shear wave velocity of soil, ν is Poisson's ratio and r_0 is the characteristic length of foundation. When the system is excited by external force, the dynamic impedance function of foundation can be estimated by the transfer function between the external force (p_{f1}(s)) and the displacement of foundation (y_{f1}(s)).This transfer function can be formulated from the mass, damping and stiffness matrices in Eq. (1)

$$K(\omega) = \frac{p_{f1}(s)}{y_{f1}(s)} = \frac{S_{11}S_{22}-S_{12}S_{21}}{S_{22}}, S_{ij} = K_s(k_{ij} - a_0^2 m_{ij} + ia_0 c_{ij}) \quad (3)$$

where m_{ij}, c_{ij}, k_{ij} are the corresponding elements of the mass, damping and stiffness matrices in Eq. (1) ignoring the unified mass, damping and stiffness, $a_0=\omega r_0/v_s$ is a dimensionless frequency parameter, and ω is the frequency of external excitation. The dynamic impedance function $K(\omega)$ is determined by m_{f1}^*, m_{f2}^*, c_{f1}^*, c_{f2}^*, c_{f3}^*, k_{f1}^*, k_{f2}^*, k_{f3}^* and K_s. To obtain a general soil-foundation model, the dynamic impedance function presented in Eq. (3) is normalized by the static stiffness

(K_s). Using the dynamic impedance function developed by Veletsos and Wei (1970) for the elastic half-plane foundation, the parameters of LPM were estimated by multiple regression analysis. The evaluated values of all parameters for this model are shown in Table 1. The comparative results of the LPM and Veletsos's analytical model presented in Fig. 2 show that LPM is suitable to represent the soil-foundation system in RTDS.

Based on LPM, The emulated system shown in Fig. 3(a) can be substructured as the RTDS system shown in Fig. 3(b). LPM model represents the soil-foundation system. The superstructure is installed on a shaking table, which is used as the transfer system to simulate the interface acceleration (a_n). As can be seen in Fig. 3(b), the interface acceleration is resulted from external excitation(r) and reaction force of superstructure (f)

$$a_n = G_{fr} r + G_{ff} f \tag{4}$$

Table 1 Parameters of the used lumped parameters model

m^*_{f1}	m^*_{f2}	c^*_{f1}	c^*_{f2}	c^*_{f3}	k^*_{f1}	k^*_{f2}	k^*_{f3}
0.033	0.003	0.501	-0.008	0.014	1.660	-0.124	0.157

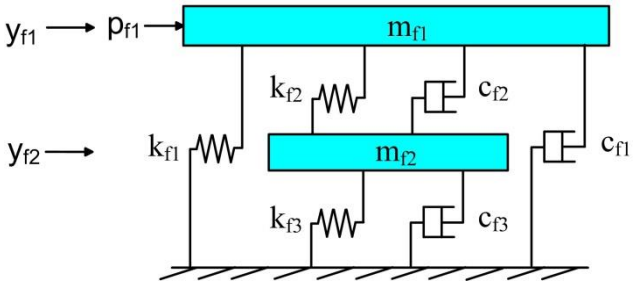

Fig. 1 Lumped parameter model

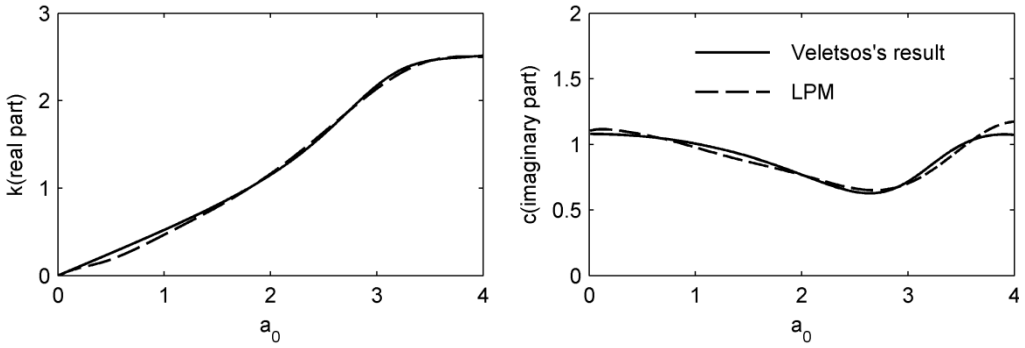

(a) real part (b) imaginary part

Fig. 2 Dynamic stiffness of elastic half-plane foundation

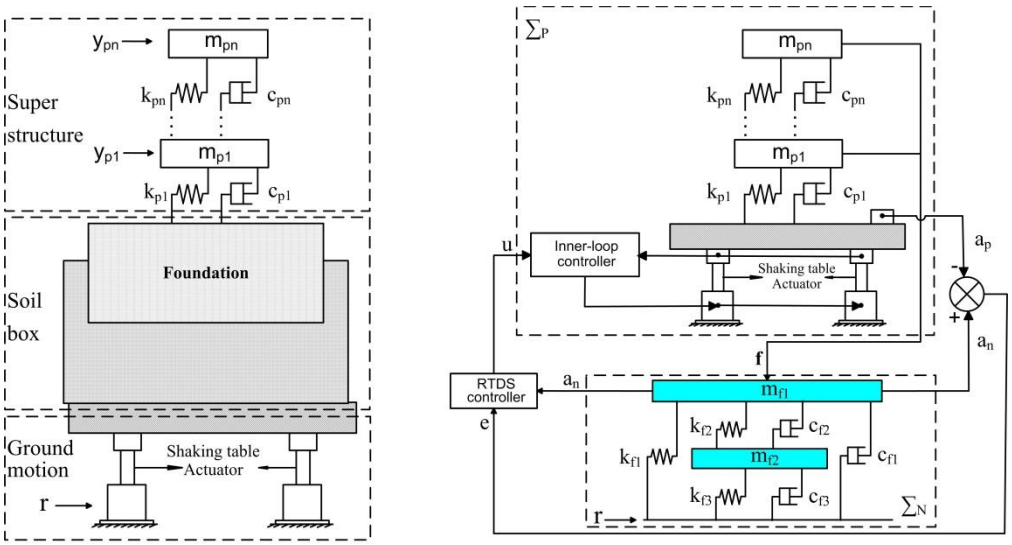

(a) Emulated system (b) Substructured system

Fig. 3 Division of the whole SSI system

From Fig. 3(b), the transfer function models for the different parts can be determined. $G_{fr}(s)$ is the transfer function between the acceleration of foundation and the external excitation, and $G_{ff}(s)$ represents the transfer function between the acceleration of foundation and the reaction force of physical substructure.

$$G_{fr}(s)=\frac{(c_{f1}s+k_{f1})(m_{f2}s^2+c_{f2}s+k_{f2})+(c_{f3}s+k_{f3})[(c_{f1}+c_{f2})s+(k_{f1}+k_{f2})]}{[m_{f1}s^2+(c_{f1}+c_{f2})s+(k_{f1}+k_{f2})][m_{f2}s^2+(c_{f2}+c_{f3})s+(k_{f2}+k_{f3})]-(c_{f2}s+k_{f2})^2} \quad (5)$$

$$G_{ff}(s)=\frac{s^2[m_{f2}s^2+(c_{f2}+c_{f3})s+(k_{f2}+k_{f3})]}{[m_{f1}s^2+(c_{f1}+c_{f2})s+(k_{f1}+k_{f2})][m_{f2}s^2+(c_{f2}+c_{f3})s+(k_{f2}+k_{f3})]-(c_{f2}s+k_{f2})^2} \quad (6)$$

Normally, the achieved value of interface acceleration is not a_n but a_p after going through shaking table because of its dynamics. That leads the needs of RTDS controller. As Tu, Lin *et al.* (2010) said, the shaking table can be approximated to a first-order system such that

$$G_s(s)=\frac{a}{s+a} \quad (7)$$

where a is the product of the time constant and the proportional gain of shaking table. And then the reaction force is formulated as

$$f(s)=G_f a_p(s) \quad (8)$$

G_f represents the transfer function of the total shear force ($f(s)$) of superstructure from excitation ($a_p(s)$), which is determined by the dynamic equation and parameters. It will be

discussed in next section.

3. RTDS control strategy for SSI systems

3.1 Modified linear substructuring control

To formulate the synthesis procedure of RTDS dynamics and control, a framework of linear substructuring controller (LSC) was proposed by Stoten and Hyde (2006), as illustrated in Fig. 4. An emulated system is conceptually decomposed into at least two substructures, $\sum_n$ and $\sum_p$. For practical cases $\sum_n$ represents the numerical model and $\sum_p$ represents the physical model. Control and excitation signals are denoted by u and r, respectively. Here, the RTDS dynamics are represented by three generalized blocks, G(s), constraint; G_1(s), excitation; and G_2(s), transfer system dynamics. G_1(s)=the relationship between the displacements of the top of the foundation (a_{nr}) and the ground motion (r); G(s) = the relationship between the control signals (u) and the acceleration of the top of the foundation (a_{nf}) from the reaction force, including the TS dynamics G_s(s), the reaction force dynamics G_f(s) and the numerical substructure dynamics G_{ff}(s);G_2(s)=the TS dynamics, thus

$$\begin{aligned} G_1(s) &= G_{fr}(s) \\ G(s) &= G_s(s)G_f(s)G_{ff}(s) \\ G_2(s) &= G_s(s) \end{aligned} \tag{9}$$

With reference to Fig. 4, the error dynamics (e= a_n-a_p) of an LSC-controlled DSS can be written as (Stoten and Hyde 2006, Stoten, Tu *et al*. 2009)

$$G_{err}(s) = \frac{G_1(s) - \left[G(s) + G_2(s)\right]K_r(s)}{1 + \left[G(s) + G_2(s)\right]K_e} \tag{10}$$

where G_{err}(s) is the transfer function between the error dynamics(e) and external excitation(r). To synchronize the two outputs $\{a_n, a_p\}$, the substructuring error is expected to equal zero, the numerator of Eq. (10) is set equal to zero, then

$$K_r(s) = \frac{G_1(s)}{G(s) + G_2(s)} \tag{11}$$

And the achieved interface acceleration (a_p(s)) resulted from external excitation(r) can be expressed as

$$G_p = \frac{a_p(s)}{r(s)} = \frac{(K_e G_1 + K_r)G_2}{1 + K_e(G + G_2)} \tag{12}$$

As known from the procedures of LSC design, the achieved interface acceleration is completely equivalent to the acceleration of the foundation in an entire system, when the models of different parts used in LSC controller are accurate. In this case, the response presented in Eq. (12) represents the acceleration of the foundation in emulated system, which can be used as the baseline for the error analysis in the following discussion.

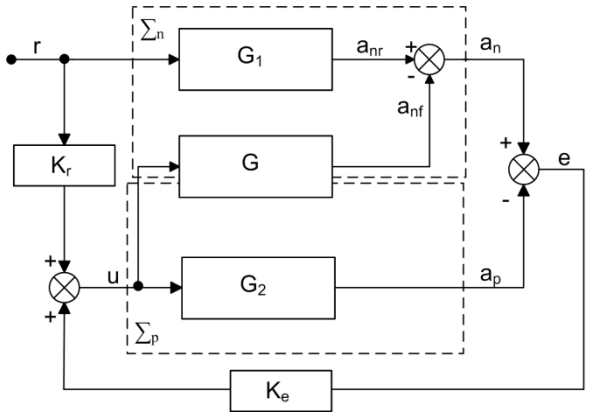

Fig. 4 Linear substructuring controller

In the design of LSC, the accurate model of numerical and physical substructure and transfer system are all needed. However, in civil engineering applications, the superstructure system has 100s of DOF, which results in three problems: (a) high orders controller for substructuring control; (b) high computation requirement for hardware used in experiment and,(c)complicated parameter identification for PS. Eq. (9) shows that the transfer function $G_f(s)$ is related to superstructures for LSC design, which represents the summation of the reaction force of all the DOFs, and the transfer function $G_f(s)$ of MDOF can be written as

$$G_f(s) = -\sum_{i=1}^{n} m_{pi} s^2 G_{pi}$$
$$G_{pi} = \frac{a_{pi}(s)}{r(s)} \tag{13}$$

where m_{pi} is the mass of i*th* DOF in *n* DOFs, G_{pi} is the transfer function between the acceleration of i*th* DOF ($a_{pi}(s)$) and the ground motion ($r(s)$). Therefore, all the parameters (mass, stiffness and damping) of superstructures are needed for the LSC design, actually, that is an overwhelming difficulty in civil engineering at present.

In the dynamic analysis of structures, the mode superposition methods (Clough and Penzien 1993) are adopted to decouple the dynamic equilibrium equations. The *n* DOFs systems are resolved into *n* SDOF systems. The response of the *n* DOFs system is then equal to the superposition of the responses of all the n SDOF systems. However, the used mode shapes need not be the exact free-vibration mode shapes for the sparse mode structure. The responses of the *n* DOFs system are exact enough when the dominant mode shapes are employed. This requires that the participating mass ratio (the ration of the participating mass to the total mass) of the included mode in the calculation of response is more than 90 percent (Wilson 2002). Thus, using mode superposition methods the modified LSC (MLSC) can be achieved, and the reaction force of PS will be

$$G_{fm}(s) = -\sum_{j=1}^{n} m_{pefcj} s^2 \frac{2\zeta_{pj}\omega_{pj} + \omega_{pj}^2}{s^2 + 2\zeta_{pj}\omega_{pj} + \omega_{pj}^2} \tag{14}$$

$$m_{pefcj} = \frac{\left(\left\{\phi_j\right\}^T \left[m_p\right] I\right)^2}{M_j}$$

$$M_j = \left\{\phi_j\right\}^T \left[m_p\right] \left\{\phi_j\right\}$$

where m_{pefcj}, ω_{pj}, ζ_{pj} are the participating mass, natural frequency and damping ratio of j*th* mode respectively , $\{\phi_j\}$ is the model shape vector of j*th* mode. $\boldsymbol{I}$ is unit vector, $[m_{\text{p}}]$ is the mass matrix of the n DOFs system (shown in Fig. 3). l is the number of the modes which satisfy the 90 percent participation rule (Wilson 2002). From Eq. (14), not all the parameters (mass, stiffness and damping) of superstructures but only the participating mass, natural frequency and damping ratio of the modes are needed for the LSC design, of which the natural frequency and damping ratio can be acquired experimentally, and the mass matrix can be readily gotten through the density and volume of the structures.

The substitution of Eq. (14) into Eq. (9) yields the block G(s) for MLSC.

$$G_m(s) = G_s(s) G_{fm}(s) G_{ff}(s) \tag{15}$$

Hence, from Eq. (11), the forward transfer function K_{r} of MLSC is

$$K_{rm}(s) = \frac{G_1(s)}{G_m(s) + G_2(s)} \tag{16}$$

The transfer function between the achieved interface acceleration (a_{p}) and external excitation(r) for the RTDS system controlled by MLSC is

$$G_{pm} = \frac{(K_e G_1 + K_{rm}) G_2}{1 + K_e (G + G_2)} \tag{17}$$

The combination of Eqs. (12) and (17) produces the relative control error resulting from MLSC

$$G_{err} = \frac{G_{pm}}{G_p} \tag{18}$$

To verify the validity of MLSC, a RTDS system is designed for the simulation of SSI. A mass-spring-damper system with two DOFs is used as the superstructure. The superstructure is constructed on the surface of a semi-infinite soil foundation. This work pays more attention to develop an accurate control strategy for SSI sub-structuring testing system. To ensure the test run in real time, the SSI effects are not expected to be very strong. Hence Poisson's ratio ν=0.25 and the mass density ρ=2000kg/m^3, the length of foundation r_0 =12m and the shear wave velocity v_{s}=200m/s are adopted. The parameter for the shaking table a=100rad/s is selected. Substituting these parameters into Eq. (2), the unified mass, stiffness, and damping of the lumped parameter model can be calculated. The parameters of this system are listed in Table 2 together with the parameters of the scaled model with the scale ratio of 1/1000, which will be used in the experimental test.

The prototype is used to illustrate the performance of MLSC firstly. From Eq. (14), the participating mass of the first mode is 2.46×10^5kg, and the total mass of this superstructure is 2.55×10^5 kg giving a participating mass ratio of 96.5%. As this is greater than 90%, a SDOF system can be used to replace the two DOFs system for the MLSC controller design. The

equivalent SDOF system will have: mass=2.46×10^5kg, natural frequency=3.3Hz, damping ration=1.3%. To ensure the stability of the RTDS-SSI system, the roots' loci method is used to select K_e. As known from the roots' loci map, the closed-loop system is unconditionally stable and the value of the feedback gain that allocates the dominant conjugate pair with a real part (arbitrarily) at s=-0.3 is found to be K_e=1.5. From Eq. (18), the MLSC control error relative to the accurately LSC control in Fig. 5 shows that the error lies in a very small frequency range near the second natural frequency of superstructure, and in this frequency band, the maximal magnitude error is less than 3%, and the maximal delay is around 80 degree. MLSC supplies adequate control accuracy relative to LSC without the limitations on the identification of all physical parameters.

3.2 The effect of the identification errors on MLSC performance

The parameters of PS and TS need to be identified before designing MLSC controller, generally, which are analysed from the response of PS and TS loading white noise or swept sinusoidal signals. Due to the complexity of the structural system, materials, dynamics of transducer and external disturbance, an error in these parameters is inevitable. Nevertheless, its effect on the linear controller is unknown. In this section, the effect of the identification errors on MLSC were analysed based on the system shown in Table 2. The relationship of the value of these parameters used in the MLSC design and the real value are assumed as

$$\begin{cases} m_{pe} = m_p + \delta_m m_p \\ \xi_{pe} = \xi_p + \delta_\xi \xi_p \\ \omega_{pe} = \omega_p + \delta_\omega \omega_p \\ a_e = a + \delta_a a \end{cases} \tag{19}$$

Table 2 Parameters of the prototype and the tested model

	Numerical substructure			Physical substructure					
	M_{fe} (kg)	C_{fe} (Ns/m)	K_e (N/m)	m_{p1} (kg)	c_{p1} (Ns/m)	k_{p1} (N/m)	m_{p2} (kg)	c_{p2} (Ns/m)	k_{p2} (N/m)
Prototype	1.58e7	2.63e8	4.39e9	1.40e5	1.72e5	1.33e8	1.15e5	1.69e5	1.55e8
Model	1.58e4	2.63e5	4.39e6	1.40e2	1.72e2	1.33e5	1.15e2	1.69e2	1.55e5

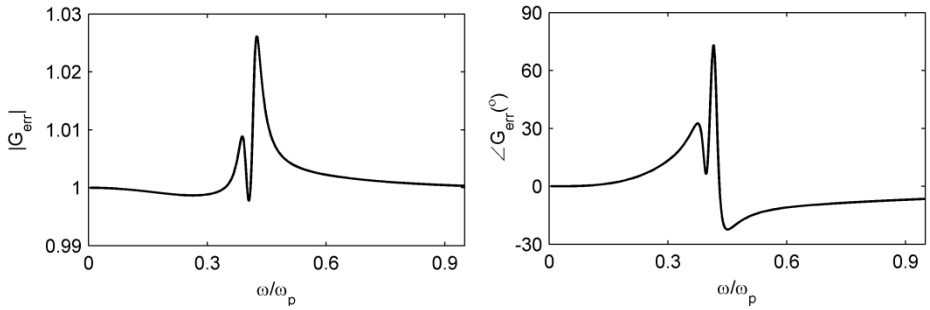

Fig. 5 Control error of MLSC

where m_{pe}, ξ_{pe},ω_{pe}, a_e are the mass, damping ratio and natural frequency of the first mode of PS, and the parameter of shaking table for MLSC design respectively, m_p, ξ_p,ω_p, a are the real value, δ_i (i=m,ξ,ω,a) are the offset ratio between designed value and real value. The substitution of Eq. (19) into Eqs. (14) and (9) produces the blocks of $\{G, G_2\}$ for MLSC design

$$\begin{aligned} G_e(s) &= G_{se}(s)G_{fe}(s)G_{ff}(s) \\ G_{2e}(s) &= G_{se}(s) \\ G_{se}(s) &= \frac{a_e}{s+a_e} \\ G_{fe}(s) &= m_{pe}s^2\frac{2\xi_{pe}\omega_{pe}s+\omega_{pe}^2}{s^2+2\xi_{pe}\omega_{pe}s+\omega_{pe}^2} \end{aligned} \tag{20}$$

The substitution of G_e(s), G_{2e}(s) in Eq, (20) into E. (11) yields the forward transfer function K_{re}

$$K_{re}(s) = \frac{G_1(S)}{G_e(S)+G_{2e}(S)} \tag{21}$$

The same as section 3.1, set K_e=1.5, then from Eq. (12). The transfer function between the achieved interface acceleration (a_p) and external excitation(r) for the RTDS system controlled by MLSC with identification error of PS and transfer system is

$$G_{pe} = \frac{(K_eG_1+K_{re})G_2}{1+K_e(G+G_2)} \tag{22}$$

Eq. (12) gives the accurate acceleration of interface from ground motion for the emulated system, the combination of Eqs. (12) and (22) produces the relative control error resulting from identification errors

$$G_{err} = \frac{G_{pe}}{G_p} \tag{23}$$

Taken the system presented in Table 2 as an example: m_p=2.46×10^{5}kg, ω_p=3.3Hz, ξ_p=1.3%, a=100rad/s, from Eq. (23), the relative control errors resulting from the identification error of m_p, ξ_p , ω_p and a individually are discussed with the offset ratio δ_i(i=m,ξ,ω,a)=±0.1, ±0.3 and±0.5 . The magnitude and phase errors caused by the identification errors of the mass, damping ratio and natural frequency of the PS, and the parameter a for shaking table dynamics are shown in Figs. 6-9.

Fig. 6 shows that the major relative error occurs near ω_p (ω_p/ω=1), for the frequency identification error with same absolute value, the relative error is symmetrical. The frequency band affected by δ_m observed from |G_{err}| is around (0.8-1.2)ω_p, while a relatively narrow frequency band of (0.85-1.05)ω_p was measured in the plot of $\angle G_{err}$. Unlike the mass identification error, for the damping identification error with same absolute value shown in Fig. 7, the relative error resulting from negative identification error is more than the positive identification error. Meanwhile, the frequency band affected by δ_ξ observed from |G_{err}| and $\angle G_{err}$ are both (0.95-1.05)ω_p, which is a more narrow range than it resulted by δ_m. As can be seen in Fig. 8, for

the frequency identification error, the positive identification error resulted in larger relative error than the negative identification error, when the identification error is small, the relative error only occurs in a small frequency range near ω_p, with the increase of δ_ω, the additionally natural frequency of physical substructure appears and the frequency band affected by δ_ω broadens. Fig. 9 shows that the identification error of shaking table deteriorates the control performance of MLSC not only near ω_p, but also with the increase of frequency of reference signals. The positive value of identification error caused much smaller relative control error than the negative value.

In general, the comparison of Figs. 6-9 revealed that, the control error of MLSC caused by the small identification error (i.e., δ_i=±0.1) is slightly and ignorable. However, when the identification error is relatively large (i.e., δ_i=±0.3 and ±0.5), Extra attention should be paid on the controller of RTDS-SSI system.

3.3 Adaptive substructuring controllers

As illustrated by the preceding section on the control errors of MLSC and the influence of identification errors on the performance of MLSC, the unknown and time-varying parameters and the uncertainties existing in the RTDS system are needed to compensate for through an adaptive controller.

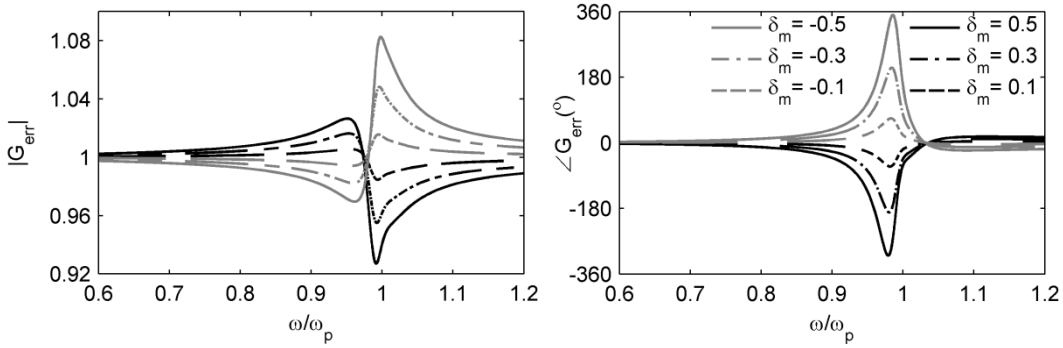

Fig. 6 Relative error resulting from identification error of PS: mass

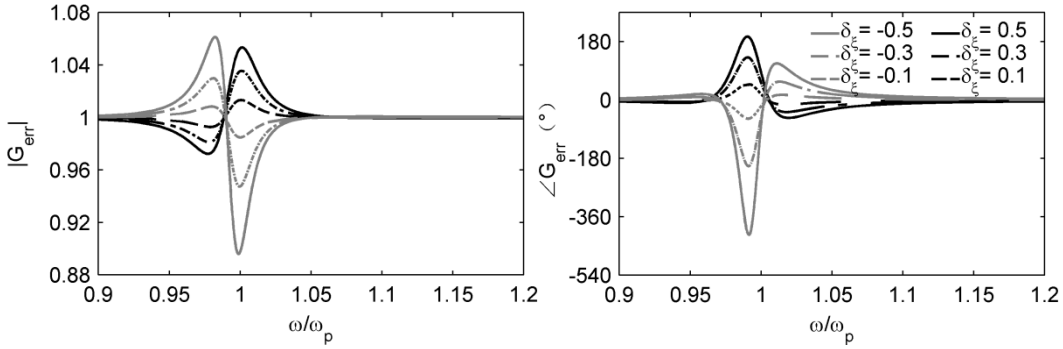

Fig. 7 Relative error resulting from identification error of PS: damping ratio

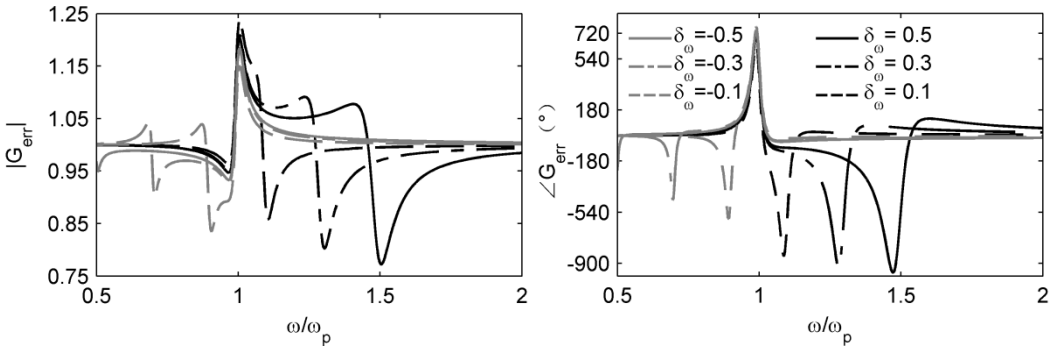

Fig. 8 Relative error resulting from identification error of PS: frequency

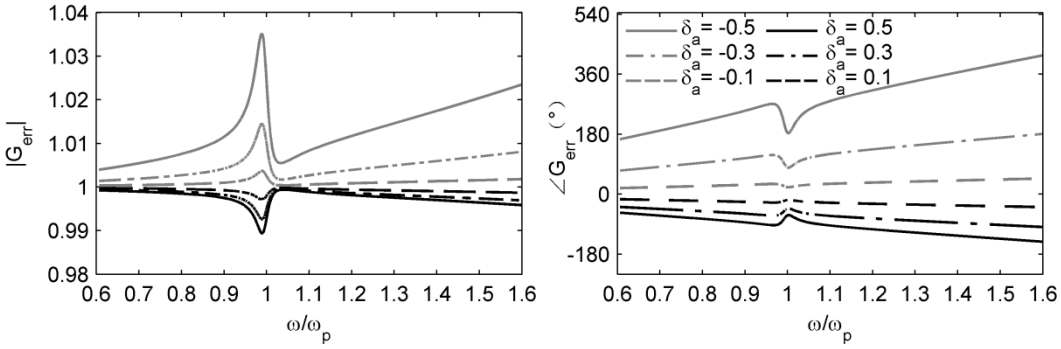

Fig. 9 Relative error resulting from identification error of shaking table

In this section, the application of the minimal control synthesis with error feedback (MCSEF) algorithm (Stoten and Hyde 2006) together with MLSC to RTDS-SSI is introduced. The MCSEF algorithm is a derivative of the adaptive minimal control synthesis (MCS) algorithm (Stoten 1989). The MCS algorithm is an adaptive model reference control strategy. The advantage of which is that the dynamics of the shaking table and the substructure are not required when designing the controller. A further potential advantage is that theoretically the controller can compensate for parameter variations. The modifications have been made to allow it to be used in substructuring (Stoten, Lim *et al*. 2007, Stoten and Hyde 2006, Stoten, Tu *et al*. 2009, Tu, Lin *et al*. 2010, Neild, Stoten *et al*. 2005). Normally, the MCS algorithm includes the reference model, so that the state error between the model and the plant is ensured to be globally asymptotically stable. In order to take full advantage of the structure of MLSC and the adaptively of MCS algorithm, the reference model of MCS has been replaced by the numerical model of RTDS (see Fig. 10).

The control signal and adaptive gains of MCSEF in Fig. 10 are generated according to the following equations

$$\begin{aligned} u(t) &= K_r(s)r(s) + K_e(s)e(s) + K_{ra}(t)r(t) + K_{ea}(t)e(t) \\ K_{ra}(t) &= \alpha\int_0^t y_e(t)r^T(t)dt + \beta y_e(t)r^T(t)dt \end{aligned} \tag{24}$$

$$K_{ea}(t)=\alpha\int_0^t y_e(t)e^T(t)dt+\beta y_e(t)e^T(t)dt$$

where $\{\alpha,\beta\}$ are adaptive weights , the ratio α=10β, which has been shown to work well empirically (Stoten, Lim *et al*. 2007), is used here. The term y_e is the output error, generated directly from e, according to $y_e(t)=C_e e(t)$,where C_e is selected to ensure a strictly positive real dynamic in the hyper stability proof for the MCSEF controller (Stoten, Lim *et al.* 2007), for first-order control, C_e is normally defined as (Stoten, Lim *et al*. 2007): $C_e=4/t_s$, where t_s is the step response time of the implicit reference model.

4. Comparative simulations

In the foregoing section, the efficacy of the MLSC algorithm with identification error of physical substructures and shaking table were demonstrated in frequency domain in terms of magnitude and phase errors. To overcome the drawback of MLSC, an adaptive control strategy called MCSEF was incorporated. In this section, as seen in Table 2, using the LPM for soil as the numerical model, the two DOFs mass-spring-damping system as the physical model, and the first-order system with a=100 rad/s as the shaking table, the performance of MLSC and MLSC-MCSEF is to be performed in time domain. The four cases comparative simulations listed in Table 3 are discussed. For the cases with identification errors, the offset ratio of the physical substructure and shaking table are made congruent (i.e., $\delta_m=\delta_\xi=\delta_\omega=\delta_a=\delta$=0.5).

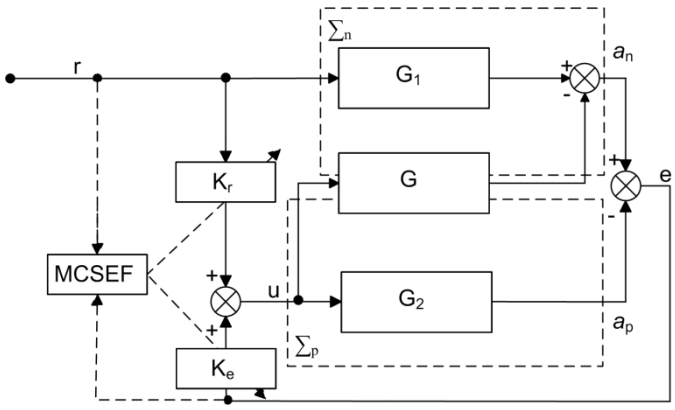

Fig. 10 MLSC-MCSEF controlled RTDS system

Table 3 Conditions for comparative simulation

Condition label	Case1	Case2	Case3	Case4
Parameters errors	None	None	$\delta_m=\delta_\xi=\delta_\omega=\delta_a=\delta$=0.5	$\delta_m=\delta_\xi=\delta_\omega=\delta_a=\delta$=0.5
Controller	LSC	MLSC	MLSC	MLSC-MCSEF

A sine sweep of amplitude 0.1 m/s^2, frequency range from 0.1 to 20 Hz and period 20s was chosen as the ground motion. The substructuring error of interface response between the emulated system and substructuring system is presented to indicate the control performance of controller for the RTDS-SSI system. Fig. 11 shows the substructuring errors of different cases together with the accurate interface acceleration response.

In Case1, the idealized model was used for numerical and physical substructure and shaking table in LSC controller design, thus, LSC produced a predictably near-perfect response, with virtually zero substructuring error (See Fig. 11(b)).

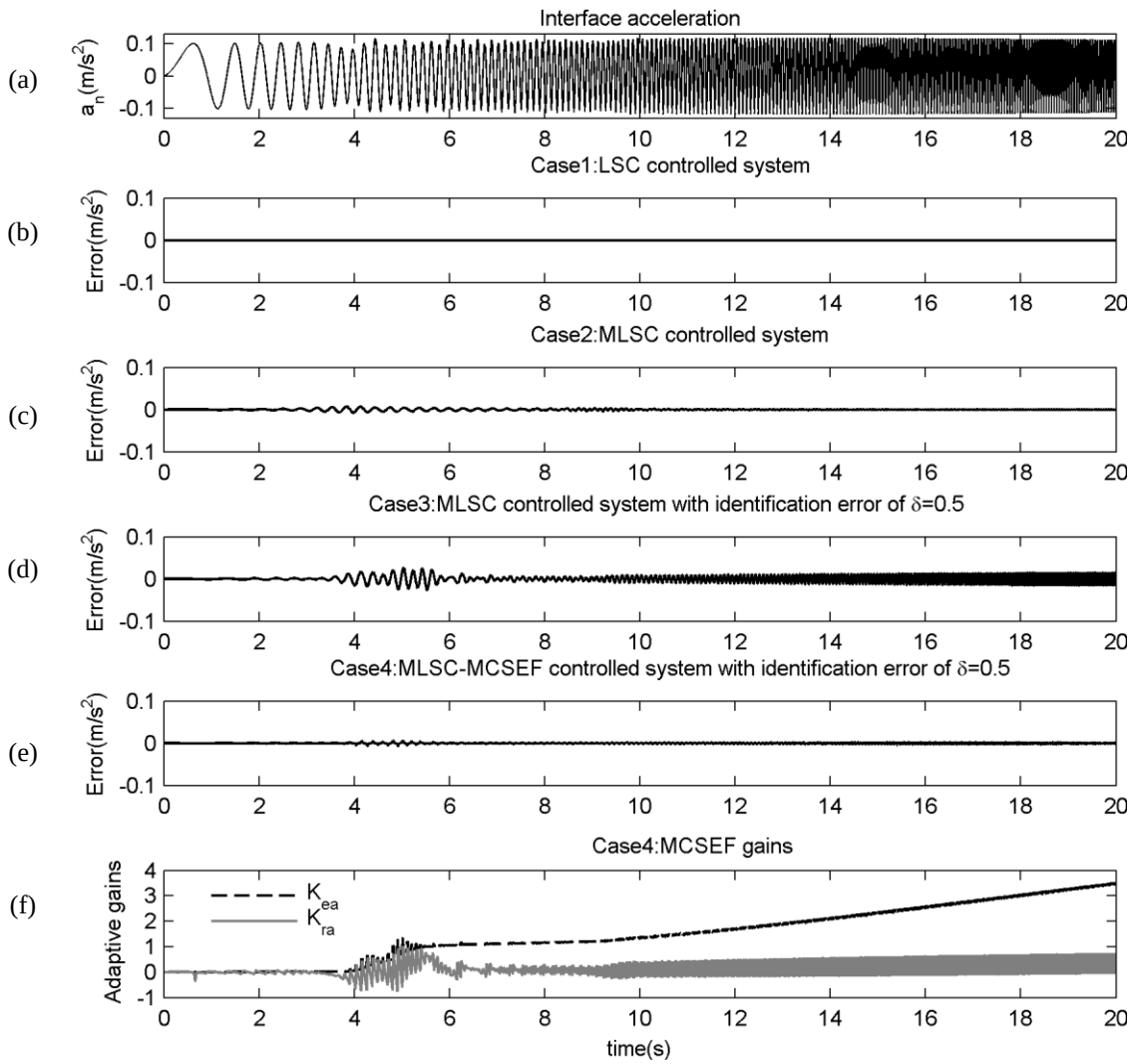

Fig. 11 Interface acceleration of RTDS-SSI system controlled by MLSC and MLSC-MCSEF

In Case 2, the RTDS-SSI system was controlled by MLSC, during the design procedures of which, the two DOFs physical substructure needed by LSC was replaced by a SDOF system with the parameters of m_p=2.46×10^{5}kg, ω_p=3.3 Hz, ξ_p=1.3%. The corresponding MLSC response in Fig. 11(c) shows a visible substructuring error between 2s to 9s (equivalent to the excitation frequency from 2 Hz to 9 Hz) that is resulted from the magnitude and phase error near the natural frequencies of the first and second mode shown in Fig. 5.

With the consideration of the identical identification error for physical substructure and shaking table in the design of MLSC in Case3, the parameters of physical substructure and shaking table become m_{pe}=3.69×10^{5}kg, ω_{pe}=4.95 Hz, ξ_{pe}=1.95% and a_e=150rad/s. The MLSC controller with identification errors produced a much larger substructuring error than the idealized MLSC as can be seen in Figs. 11(c) and 11(d). In this case, substructuring error includes two parts. One part lies in the range between the two natural frequencies of physical substructure (3.3 Hz-8.76 Hz) as shown in Fig. 6 to Fig. 8, which appears around 2s to 9s in Fig. 11(d). It is resulted from the parameter error of physical substructure. The other part lies in the range over 9s equivalent to more than 9 Hz is caused by the parameter error of shaking table as can be seen in Fig. 9.

However, as was seen in section 3.3, the adaptive MLSC incorporating MCSEF strategy would be expected to melt the substructuring error caused by MLSC and identification error. This expectation is put to Case 4. The initial conditions of which are as follows: α=1000, β=100 and t_s=0.01s, a process based on empirical selection, as described by Stoten and Benchoubane (1990). The substructuring responses are as shown in Fig. 11(e), which are virtually identical to those in Fig. 11(b). The adaptive gains of MCSEF in Fig. 11(f) varying with the substructuring error shown in Fig. 11(d) demonstrates that MLSC-MCSEF has displayed good adaptability to the identification error.

5. Experimental tests

In this section, the performance of RTDS system controlled by MLSC and MLSC-MCSEF was evaluated in an authentic experiment. Based on the authentic testing system, the effect of SSI on frame structure was checked roughly.

5.1 Physical substructure

The parameters of prototype structure listed in Table 2 were scaled in scale ratio 1:1000 in the experimental test. The scaled parameters of physical and numerical substructure were also presented in Table 2. Based on the scaled model, a two-story steel frame as shown in Fig. 12 was constructed. For each story, four cold formed steel members with angle section and a steel plate with additional mass-blocks were used.

Before conducting RTDS test, a conventional shaking table test with white noise excitation was carried on to identify the dynamic parameters of the physical substructure. The acceleration spectrums of top story were shown in Fig. 13. As can be seen, the frequencies of the first and second mode were 3.235 Hz and 8.469 Hz, which were close to the designed values of 3.3 Hz and 8.76 Hz respectively. For the design of MLSC controller in this test, the modal damping ratio and mass of the first mode were also needed. Estimating from the measured acceleration of the top and bottom story, the damping ratio of the first mode was1.94%, and the corresponding model shape vector was $[1\ 0.483]^T$. Substituting the two values into Eq. (14) gave the model mass of 226 kg.

Fig. 12 Physical substructure used in the test

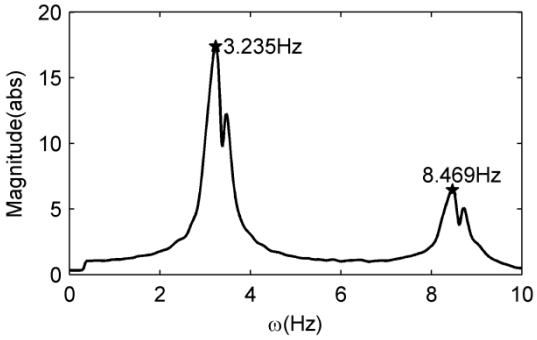

Fig. 13 Acceleration spectrum of top story

Compare with the designed value of the mass, damping ratio and frequency of the first mode: 246kg, 1.3% and 3.3Hz, the identified results leaded -8%, 46% and -2% error for the mass, damping ratio and frequency. Based on the analytical results in Section 3.2, the identification error of damping ratio may cause remarkable control error in MLSC relative to mass and frequency.

5.2 RTDS test for the simulation of SSI

The efficiency of LPM to describe the properties of soil-foundation system has been verified by Wang, Wang *et al.* (2011) using finite element model. And in their studies, the simulation of SSI using RTDS also has been implemented successfully. In this work, a larger physical substructure and a shaking table with more complicated dynamics, which gives greater challenge for RTDS control, was used. The tested models of physical and numerical substructure have been listed in Table 2. The shaking table used here is controlled by three-variable controller. The estimated parameter of the shaking table used in MLSC design was a=100rad/s. A seismic wave measured from Kobe Earthquake (see Fig. 14) was selected as the input excitation of the SSI system. In the implementation of this test, the reaction force of the physical substructure was represented by the total inertia force of the lumped mass of each story, which was the product of the absolute acceleration and the mass of each story.

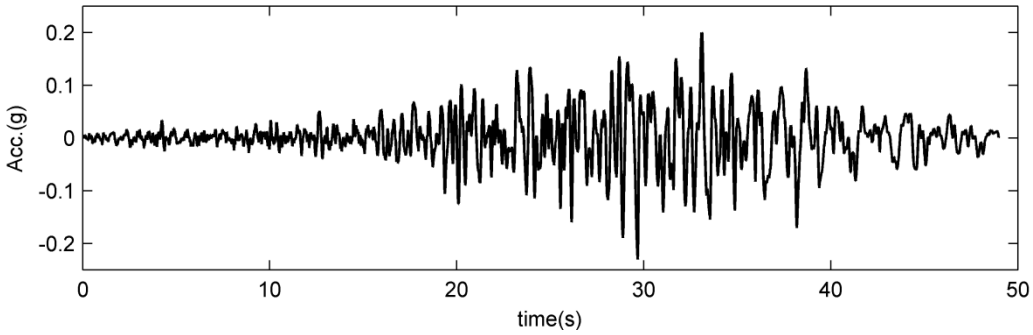

Fig. 14 Seismic wave used in the test

In the experiment, the MLSC and MLSC-MCSEF controlled RTDS-SSI tests were conducted for comparison. Fig. 15 displayed the desired and achieved acceleration of shaking table in the form of synchronization subplots. It was seen that MLSC supplied an acceptable accuracy for RTDS-SSI test. After using MLSC-MCSEF, the agreement of the desired and achieved response was improved further as shown in Figs. 15(a) and 15(b), because MCSEF can track and correct the parameters error, uncertainties and other disturbance existing in the operation of test. That was verified by the adaptive gains of MCSEF shown in Fig. 15(c).

To evaluate the effect of SSI on the dynamic response of frame structure, the soft soil foundation system with the shear wave velocity v_s=200m/s was tested using the MLSC-MCSEF controlled RTDS. For comparison, the hard soil foundation system was also tested using the conventional shaking table test without the consideration of SSI. The tested results of acceleration and displacement response from 22s to 32s were shown in Fig. 16. In general, the SSI effect reduced both the relative acceleration and displacement of structure. The reduction ratio of acceleration for bottom and top story was around 14% and 18% respectively, while the corresponding value of displacement was around 16% and 17%. It was obvious that the SSI effect had less influence on the lower story than the upper story for the frame structure.

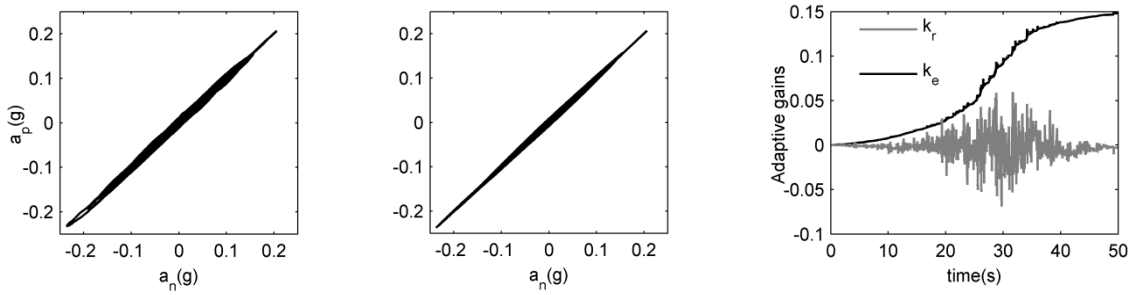

(a) a_p vs a_n controlled by MLSC (b) a_p vs a_n controlled by MLSC-MCSEF (c) Adaptive gains of MCSEF

Fig. 15 Control performance of RTDS-SSI system

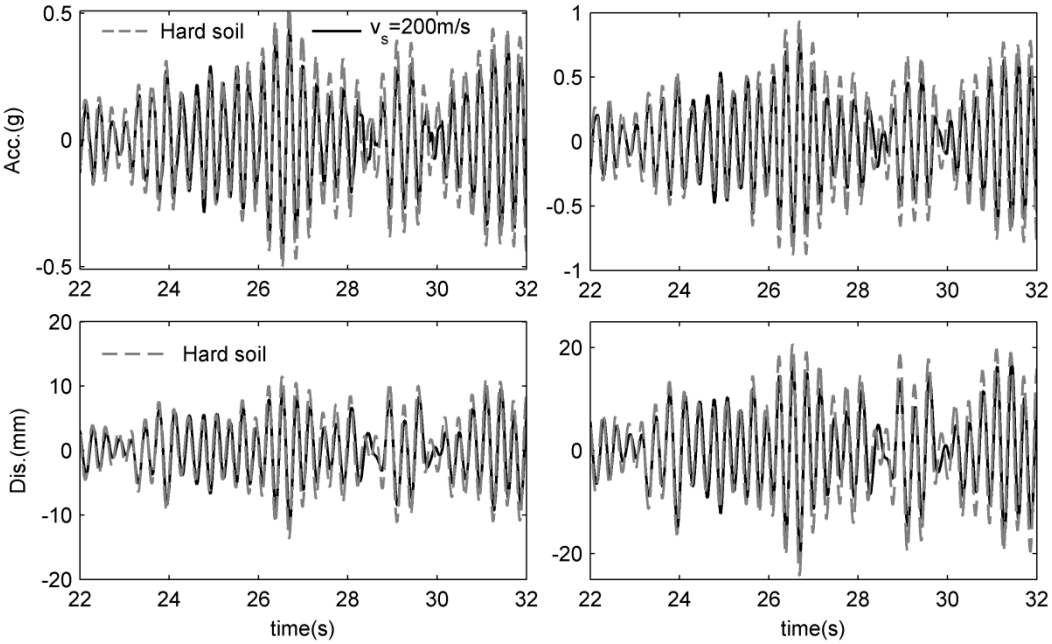

(a) Bottom story (b) Top story

Fig. 16 Structural response comparison with and without soil-structure interaction

6. Conclusions

The huge size and weight of structures make it difficult to test large size SSI system experimentally, together with soil. Establishing a framework for the application of real-time dynamically substructured systems to SSI system enables the large size or even prototype tests to be possible, which built a bridge between the theoretic and testing research for SSI.

The complexity of structures in civil engineering cannot give an accurately mathematical model using limited DOFs for the physical model needed for linear substructuring controller. For this problem, the modified linear substructuring controller was proposed based on the mode superposition methods. It was found that the physical model for MLSC design was simplified greatly, while the control performance of MLSC was still reasonable.

The adaptability of MLSC to identification error of physical substructure and shaking table, due to the complexity of the structural system, materials, dynamics of transducer and the external disturbance, was analysed. The results showed that MLSC had good robustness to these identification errors when their values are not too large (i.e., less than 10%), while when the values of these identification errors were relative large, extra controller was needed to handle the control error.

An adaptive control algorithm (MCSEF) incorporating with MLSC was synthesized to deal with these identification errors which are intractable for MLSC. The simulated showed that MLSC-MCSEF controlled RTDS-SSI system produced a good response, with negligible substructuring error even when the identification error of physical substructure and shaking table was large (i.e., 50%). Finally, an experimental test verified that MLSC-MCSEF supplied a

successful control strategy for RTDS-SSI system.

Acknowledgments

The authors gratefully acknowledge the support of the Beijing Natural Science Foundation (8164050) in the pursuance of this work.

Reference

Chatzigogos, C.T., Pecker, A. and Salencon, J. (2009), "Microelement modeling of shallow foundations", *Soil Dyn. Earthq. Eng*., **29**(6), 765–781.

Chen, C. and Ricles, J.M. (2009), "Improving the inverse compensation method for real-time hybrid simulation through a dual compensation scheme", *Earthq. Eng. Struct. D.*, **38**(10), 1237-1255.

Chen, P.C., Chang, C.M., Spencer, Jr., B.F. and Tsai, K.C. (2015), "Adaptive model-based tracking control for real-time hybrid simulation", *Bull. Earthq. Eng.*, **13**(6), 1633-1653.

Chen, Y.Q., Lü, X.L. et al. (2006), "Comparative study on the dynamic soil-structure interaction system with various soils by using shaking table model tests", *China Civil Eng. J.*, **39**(5), 57-64. (in Chinese)

Clough, R.W. and Penzien, J. (1993), *Dynamics of Structures*, McGraw-Hill Education, New York, USA.

Enokida, R., Stoten, D. and Kajiwara, K. (2015), "Stability analysis and comparative experimentation for two substructuring schemes, with a pure time delay in the actuation system", *J. Sound Vib.*, **346**, 1-16.

Heath, A., Darby, A.P. and Bawcombe, J. (2008), "Substructure testing for dynamic soil-structure interaction", *Proceedings of the 2nf British Geotechnical Association International Conference on Foundations–ICOF*, Garston, Watford, UK, June.

Heath, A., Darby, A.P. and Bawcombe, J. (2008), "Substructure testing for dynamic soil-structure interaction", *Proceedings of the 2nd British Geotechnical Association International Conference on Foundations - ICOF 2008*.

Horiuchi, T. and Konno, T. (2001), "A new method for compensating actuator delay in real-time hybrid experiments", *Philos. T. Roy. Soc. London Series A - Mathematical Physical and Engineering Sciences*, **359**(1786), 1893-1909.

Horiuchi, T., Inoue, M., Konno, T. and Namita, D.Y. (1999), "Real-time hybrid experimental system with actuator delay compensation and its application to a piping system with energy absorber", *Earthq. Eng. Struct. D.*, **28**(10), 1121-1141.

Konagai, K. and Ahsan, R. (2002), "Simulation of nonlinear soil-structure interaction on a shaking table", *J. Earthq. Eng.*, **6**(1), 31-51.

Luan, M.T. and Lin, G. (1996), "2 DOF lumped parameter model of dynamic impedances of foundation soils", *J. Dalian Univ. Technol.*, **36**(4), 477-482. (in Chinese)

Medina, C., Aznarez, J.J., Padron, L.A. and Maeso, O. (2013), "Effects of soil-structure interaction on the dynamic properties and seismic response of piled structures", *Soil Dyn. Earthq. Eng.*, **53**, 160-175.

Mylonakis, G. and Gazetas, G. (2000), "Seismic soil-structure interaction: beneficial or detrimental", *J. Earthq. Eng.*, 4(3), 277-301.

Nakashima, M., Kato, H. and Takaoka, E. (1992), "Development of real-time pseudo dynamic testing", *Earthq. Eng. Struct. D.*, **21**(1), 79 -92.

Neild, S.A., Stoten, D.P., Drury, D. and Wagg, D.J. (2005), "Control issues relating to real-time substructuring experiments using a shaking table", *Earthq. Eng. Struct. D.*, **34**(9), 1171-1192.

Pitilakis, D., Dietz, M., Wood, D.M., Clouteau, D. and Modaressi, A. (2008),"Numerical simulation of dynamic soil-structure interaction in shaking table testing", *Soil Dyn. Earthq. Eng.*, **28**(6), 453-467.

Shang, S.P., Zhang, J.S. et al. (2007), "Test study of the dynamic interaction of structure-box foundation-soil system", *J. Hunan University* (Natural Sciences), **4**(1), 1-4. (in Chinese)

Stoten, D.P. (1989), "A minimal controller synthesis adaptive algorithm for environmental systems", *Science et Technique du Froid*, 52(3), 277-286.
Stoten, D.P. and Benchoubane, H. (1990), "Robustness of a minimal controller synthesis algorithm", *Int. J. Control*, **51**(4), 851-861.
Stoten, D.P. and Hyde, R.A. (2006), "Adaptive control of dynamically sub structured systems: the single-input, single-output case", *Proc. IMechE, Part I: J. Systems and Control Engineering*, **220**(1), 63-79.
Stoten, D.P., Lim, C.N. and Neild, S.A. (2007), "Assessment of controller strategies for real-time dynamic substructuring of a lightly damped system", *Proceedings of the Institution of Mechanical Engineers, Part I: Journal of Systems and Control Engineering*, **221**(12), 235-250.
Stoten, D.P., Tu, J.Y. and Li, G. (2009), "Synthesis and control of generalised dynamically substructured systems", *Proceedings of the Institution of Mechanical Engineers, Part I: Journal of Systems and Control Engineering*, **223**(13), 371-392.
Tu, J.Y., Lin, P.Y., Stoten, D.P. and Li, G. (2010), "Testing of dynamically substructured, base-isolated systems using adaptive control techniques", *Earthq. Eng. Struct. D.*, **39**(6), 661-681.
Veletsos, A.A. and Wei, Y.T. (1970), "Lateral and rocking vibrations of footings", *J. Soil Mech. Found. Div. - ASCE*, **97**(9), 1227-1249.
Wallace, M.I., Wagg, D.J. and Nelld, S.A. (2005), "An adaptive polynomial based forward prediction algorithm for multi-actuator real-time dynamic substructuring", *Proceedings of the Royal Society A-Mathematical Physical and Engineering Sciences*, **461**(2064), 3807-3826.
Wang, Q., Wang, J.T., Jin, F., Chi, F.D. and Zhang, C.H. (2011), "Real-time dynamic hybrid testing for soil–structure interaction analysis", *Soil Dyn. Earthq. Eng.*, **12**(31), 1690-1702.
Wilson, E.L. (2002), *Three-Dimensional Static and Dynamic Analysis of Structures*, Computers and Structures, Inc. Berkeley, California, USA.
Wolf, J.P. (1985), *Dynamic Soil-Structure Interaction*, Prentice Hall, Englewood Cliffs, New Jersey, USA.
Yan, X.Y., Li, Z.X., Han, Q. and Du, X.L. (2014), "Shaking tables test on long-span rigid-framed bridge considering soil-structure interaction", *J. Eng. Mech. - ASCE*, **31**(2), 58-64. (in Chinese)
Zhu, F., Wang, J.T., Jin, F., Gui, Y. and Zhou, M.X. (2014), "Analysis of delay compensation in real-time dynamic hybrid testing with large integration time-step", *Smart Struct. Syst.*, **6**(14), 1269-1289.

BS